Journal of Molecular Structure 1236 (2021) 130228

Contents lists available at ScienceDirect

Journal of Molecular Structure

journal homepage: www.elsevier.com/locate/molstr

Cis and *trans* isomers of 1-(5-bromothiophen-2-yl)-3-(10-chloroanthracen-9-yl)prop-2-en-1-one: Synthesis and characterization

P. Naresh [a,1], B. Pramodh [b,1], S. Naveen [c,1,*], S. Ganguly [d], J. Panda [e], K. Sunitha [a], W. Maniukiewicz [f], N.K. Lokanath [b,*]

[a] GITAM Institute of Pharmacy, GITAM University, Rushikonda, Visakhapatnam, 530 045, India
[b] Department of Studies in Physics, Manasagangotri, University of Mysore, Mysuru, 570 006, India
[c] Department of Physics, Faculty of Engineering & Technology, JAIN (Deemed-to-be University), Jain Global Campus, Ramanagara Dist., 562 112, India
[d] Department of Pharmaceutical Sciences and Technology, Birla Institute of Technology, Mesra, Ranchi, 835 215, Jharkhand, India
[e] Raghu College of Pharmacy, Dakamarri, Bheemunipatnam, Visakhapatnam, 531 162, India
[f] Institute of General and Ecological Chemistry, Department of Chemistry, Lodz University of Technology, Zeromskiego 116, 90-924 Lodz, Poland

ARTICLE INFO

Article history:
Received 23 December 2020
Revised 25 February 2021
Accepted 26 February 2021
Available online 12 March 2021

Keywords:
Chalcone
X-ray diffraction
Cis-trans isomers
Hirshfeld surface
Energy framework

ABSTRACT

Chalcone derivatives are simple chemical scaffold found in natural products and have been extensively used as an effective template in medicinal chemistry for drug discovery. Two new geometrical isomers of 1-(5-bromothiophen-2-yl)-3-(10-chloroanthracen-9-yl)prop-2-en-1-one were synthesized, isolated and characterized by various spectroscopic techniques (FT-IR, NMR, LC-MS and UV-visible). Two different shaped (*cis* and *trans*) yellow colored single crystals were obtained by slow evaporation method and the molecular structures were confirmed by X-ray diffraction studies. The *cis* configuration crystallizes in the monoclinic $P2_1/c$ space group, whereas, *trans* configuration crystallizes in the orthorhombic $P2_12_12_1$ space group. The conformational changes lead to variations in molecular packing arrangement. In *cis*, 2-D layer-like architecture is constructed by C-H…O and S…S contacts, whereas, in *trans* 3-D zig-zag pattern is generated by C-H…O, C-H…Cl and Br…π interactions. The unique supramolecular topology of the isomers established by diverse intra and intermolecular interactions was analysed by Hirshfeld surfaces, 2D fingerprint plots, 3D energy framework and NCI index model. The Frontier molecular orbitals explored HOMO-LUMO energy gap and associated electronic properties were calculated. The molecular electrostatic potential (MEP) was plotted to identify the reactive sites in the molecule.

1. Introduction

Thiophene chalcones and their derivatives have received a great deal of endorsement due to their relatively simple structures with diverse pharmacological [1–3] and nonlinear optical properties [4]. These derivatives exhibit many interesting properties in dye chemistry [5], conductivity based sensors [6,7], electronic and optoelectronic devices [8,9], and also in corrosion inhibition [10]. Recently, materials with non-linear optical properties in the near-infrared region have been exploited due to their potent applications in optical communication, optical data processing and storage, 3D microfabrication, optical power limiting and bio-imaging [11–14]. On the other hand, polyaromatic hydrocarbons containing π-conjugated structures like anthracene, having three six-membered rings fused together in a planar-like arrangement known to show unique properties in terms of conductivity that have led to significant advancements in the field of organic electronics [15–22]. Due to its high fluorescence and quantum yield from the strong-conjugated and rigid structure, anthracene has become a star building block in organic light-emitting diodes [23,24]. Moreover, chemical modifications on anthracene would tune the molecular packing and charge transport properties, and fortunately, attaching the aryl groups, like phenyl, naphthyl, thienyl, and bithiophene units [25] to anthracene at active end and peri positions could extend the π-system very easily and enhances the nonlinear optical properties [26]. Recently, Zainuri *et.al* [27], found that the presence of anthracene fused ring system and the halogen phenyl substituent at the terminal ring

* Corresponding authors.
E-mail addresses: s.naveen@jainuniversity.ac.in (S. Naveen), lokanath@physics.uni-mysore.ac.in (N.K. Lokanath).
[1] These authors contributed equally

https://doi.org/10.1016/j.molstruc.2021.130228
0022-2860/

derivatives is useful in getting good quality single crystal with enhanced NLO properties. Thiophene and anthracene oligomers and polymers are also investigated for luminescence, semiconductor and sensing properties [28–30]. Therefore, based on the extensive literature and understandings we merged systematically the above two heterocyclic ring moieties with one single chalcone for attaining efficient hybrid organic.

Polymorphism has seized the attention of a crystal engineers due to its significantly different physicochemical properties and potential applications in the discovery of drugs, explosives, dyes and pigments. Moreover, polymorphs are valuable for understanding the relationship of crystal packing and structure property [31–34]. Crystal habit of crystalline material is governed by its internal structure, molecular packing and intermolecular interactions and that can affect many properties such as, filtration, drying, compression, tableting, flow characteristics and the dissolution rate of a drug. Owing to the better manufacturability characteristics, ease of handling and stability of solids, they are most preferable for the development of drugs over a solution or semisolid formulation. A comprehensive understanding of the crystalline forms of all the materials involved in drug formulation is very crucial for successful drug development [35–38].

The reports on the analysis of effects of *cis* and *trans* configurations of chalcones on the biological applications are very rare. Herein, we report the synthesis and spectroscopic characterization of a novel chalcone derivative. Interestingly, *cis* and *trans* conformers of title compound are confirmed by single crystal X-ray diffraction method. The structure conformational diversity and crystal packing modes of both the forms are studied using crystallographic and quantum computational methods. Further, DFT calculations are performed to understand the electronic properties of the *cis* and *trans* isomers.

2. Experimental section

2.1. Materials and methods

The ketone (2-acetyl-5-bromo-thiophene) and the aldehyde (10-chloro-anthracen-9-aldehyde) were purchased from Sigma Aldrich and Merck, India. Lithium hydroxide monohydrate ($LiOH{\cdot}H_2O$) was procured from Sisco Research Laboratories, India. All the reagents were used without purification and solvents used were of analytical grade. The solvent system used for column chromatography was *n*-hexane: ethyl acetate (8:2). Sonication was performed using an ultrasonic cleaner (with a frequency of 50 Hz and a nominal power of 170 W). The IR spectra of synthesized titled compounds were taken on Bruker FTIR spectrophotometer. ^1H and ^{13}C NMR spectra were recorded on Bruker Avance DRX400 (400 MHz for ^1H NMR and 100 MHz for ^{13}C NMR) in $CDCl_3$ solvent. Chemical shifts were reported as δ (ppm) relative to TMS as internal standard. Coupling constants J are expressed in Hertz. Mass spectra was recorded on Agilent 6545 Q-TOF LC/MS.

2.2. Synthesis of 1-(5-bromothiophen-2-yl)-3-(10-chloroanthracen-9-yl) prop-2-en-1-one (3)

A mixture of 2-acetyl-5-bromo-thiophene (1) (1 g, 4.85 mmol), 10-chloro-anthracen-9-aldehyde (2) (1.16 g, 4.85 mmol) in methanol (25 mL) was treated with lithium hydroxide monohydrate ($LiOH{\cdot}H_2O$) (20 mg, 0.485 mmol). The reaction pathway is as shown in Scheme 1. The mixture was irradiated in a water bath of an ultrasonic cleaner at room temperature for 15 minutes. The reaction mixture was then poured over crushed ice, acidified with dilute HCl and the resulting solid product was collected by filtration, washed with cold water and dried. The residue was purified on column chromatography (n-hexane: ethyl acetate, 8:2) to afford pure yellow crystals [39,40]. After being kept at room temperature in light for few days until the solvent was evaporated, single crystals of (3) trans-*E* and *Z*-*cis* isomers (Fig. 2) grew on the bottom of the glass crystallizer and these isomers were separated manually with a pair of tweezers. During the crystallization process, we have observed different sizes and shapes of yellow colored crystals, which were formed in the glass crystallizer, are shown in supplementary Fig. S6. Single crystal X-ray crystallography studies on different type of crystals confirms the *cis* and *trans* isomers of the novel chalcone derivatives, 1-(5-bromothiophen-2-yl)-3-(10-chloroanthracen-9-yl) prop-2-en-1-one (3).

2.4. Single crystal X-Ray diffraction studies

Crystals suitable for X-ray crystallography were selected using an optical microscope. The X-ray diffraction data were collected at room temperature by the ω-scan technique using Rigaku XtaLAB Mini CCD diffractometer equipped with X-ray generator operating at 50 kV and 12 mA, CCD area detector and fine-focus sealed tube with a graphite monochromator using MoKα (λ = 0.71073 Å) radiation. Data were collected with χ fixed at 54°, for different settings of φ (0° and 360°), keeping the scan width of 0.5° with exposure time of 4 s and the sample to detector distance was fixed to 50 mm. Data collection and reduction were performed using *CrystalClear* program [41]. The structure was solved by direct methods with *SHELXS* [42] and refined by a full-matrix least-squares technique on F^2 using *SHELXL*-2014 [43,44] with anisotropic thermal parameters for the non-H atoms. All the hydrogen atoms were located using difference Fourier techniques and refined with isotropic temperature factors. Molecular graphics were generated using *Mercury* 4.0 program [45]. The crystal data and structure refinement details are given in Table 1.

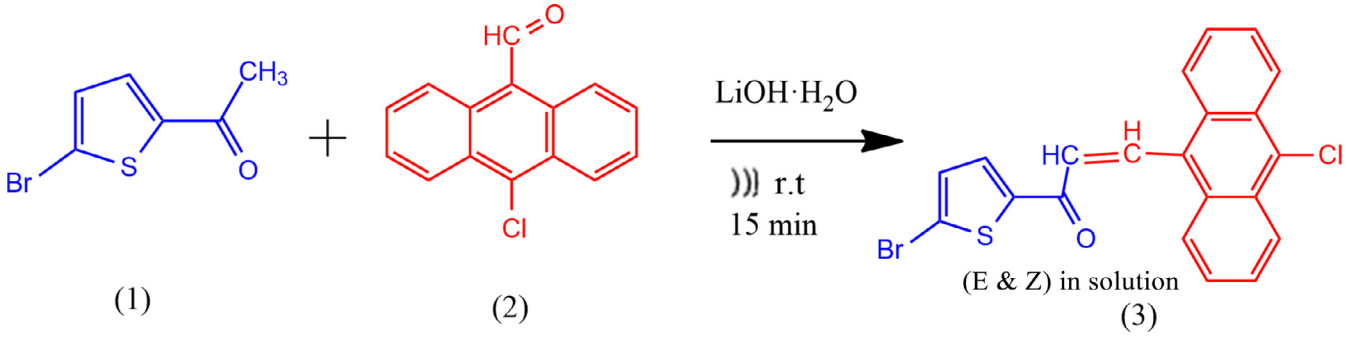

Scheme 1. Schematic representation of synthesis of 1-(5-bromothiophen-2-yl)-3-(10-chloroanthracen-9-yl) prop-2-en-1-one.

Table 1
Crystal data and structure refinement details.

Parameter	cis	Trans
CCDC deposit No.	1522484	1960503
Empirical formula	$C_{21}H_{12}BrClOS$	$C_{21}H_{12}BrClOS$
Formula weight	427.73	427.73
Temperature (K)	296(2)	293(2)
Radiation	MoKα	MoKα
Wavelength (Å)	0.71073	0.71073
Crystal system	Monoclinic	Orthorhombic
space group	$P2_1/c$	$P2_12_12_1$
a (Å)	12.3913(14)	5.6210(6)
b (Å)	12.9272(13)	16.8730(19)
c (Å)	11.0174(13)	18.5200(2)
α (°)	90.00	90.00
β (°)	96.135(4)	90.00
γ (°)	90.00	90.00
Volume (Å^3)	1754.7(3)	1756(3)
Z	4	4
Density(calculated) Mg m^{-3}	1.619	1.617
Absorption coefficient mm^{-1}	2.620	2.616
F_{000}	856	856
Crystal size (mm)	0.120×0.12×0.120	0.220×0.220×0.22
θ range for data collection	2.28° to 27.24°	3.27° to 27.50°
Index ranges	$-15\leq h\leq 15$ $-16\leq k\leq 16$ $-14\leq l\leq 14$	$-7\leq h\leq 2$ $-6\leq k\leq 21$ $-12\leq l\leq 24$
Reflections collected	43962	3836
Independent reflections	3903 [R_{int} = 0.0555]	3452 [R_{int} = 0.1397]
Absorption correction	multi-scan	multi-scan
Refinement method	Full matrix least-squares on F^2	Full matrix least-squares on F^2
Data / restraints / parameters	3903/0/226	3452/0/227
Goodness-of-fit	1.054	0.952
R1, wR2 [$I > 2\sigma(I)$]	0.0367, 0.0730	0.0688, 0.1677
R1, wR2 [all data]	0.0601, 0.0806	0.0856, 0.1802
Residual (eÅ^{-3})	0.365 and −0.494	1.145 and -0.878

2.5. Theoretical calculations

2.5.1. Hirshfeld surface analysis

The Hirshfeld surface analysis helps to explore the intermolecular interactions in crystal as they provide a visual picture of molecular shape in a crystalline environment. It identifies different types of inter-contacts with color coding distance from the nearest atom exterior (d_e) and interior (d_i) to the surface. The spherical atom electron densities were used to calculate the electron distribution based on which the 3D molecular Hirshfeld surfaces in the crystal structure were constructed. The 2D finger print plot analysis provides contributions of different intermolecular interactions of the compound in crystalline environment quantitatively. The d_e and d_i distance scales are displayed on the graph axes in the range of 0.6 to 2.8 Å. The Hirshfeld surfaces are mapped with d_{norm} and 2D finger print plots are generated and visualized using *Crystal Explorer* 17.5 [46]. Further, the intermolecular interaction energies between the molecular pair of clusters of fragments within radius of 3.8 Å was calculated using *Crystal Explorer* 17.5. The 3D topology of the predominant interactions involved in crystal packing is visualized through energy frameworks based on the calculated interaction energy values [47,48].

2.5.2. Quantum computational studies

The quantum chemical calculations and spectroscopic assignments of the compounds were made using density functional theory (DFT). The coordinates of the compounds were optimized in gas phase using DFT/B3LYP hybrid functional calculations with 6-311+G (d, p) level basis set. The frontier molecular orbitals, their energy gap (HOMO-LUMO) and the related local and global indexes (electro negativity, chemical potential, hardness, softness, electrophilicity) were estimated using Koopman's approximation [49,50]. Further, the calculated molecular electrostatic potential (MEP) and natural atomic charges of the compounds were estimated to identify the possible reactive sites within the molecular system. All the above theoretical calculations were carried out using *Gaussian* 16 package [51] and visualized using *Gaussview* 6.0.16 without any geometrical constraints [52]. Furthermore, non-covalent interaction between the fragments of *cis* and *trans* isomers were determined and analyzed within the framework of Bader's quantum theory of atoms in molecules (QTAIM), non-covalent interactions index (NCI) model and the nature of various interactions are represented by 2-D scatter plot. QTAIM analysis were carried out using Multiwfn 3.6 software [53] on the wave functions generated by DFT at the B3LYP level.

3. Results and discussion

3.1. Conformational properties of chalcones

Chalcones are flexible molecules capable of existing in various conformations and their properties depend on a suitable ring substitution and the presence of α,β-unsaturated ketone moiety [54]. Chalcones exist as either *E*-(*trans*) or *Z*-(*cis*) isomers (Fig. 1). The *E*-isomer is the thermodynamically most stable form in most cases, so the *E* isomer is isolated as the majority of the chalcones [55]. Configuration of *Z* isomer is unstable due to the strong steric effects between the carbonyl group and phenyl-ring. While *E* and *Z* mixtures exist in solution, the *E*-form invariably results on crystallization. So, recrystallization of an *E–Z* mixture yields *E* isomer as the only stereoisomer [56–58].

3.2. Spectral characterization of the title compound (3)

Structural characterization of the title compound (3) was carried out by FTIR, **UV-visible, NMR and LC-MS spectral analy-**

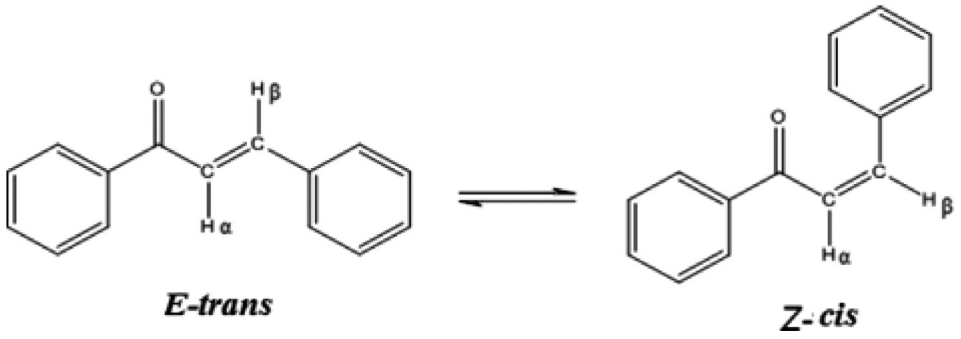

Fig. 1. *E* and *Z* conformations of Chalcones.

sis. The experimental FT-IR spectra of the title chalcone confirms the functional groups and the carbonyl stretching vibrations appearing in the region 1750-1660 cm^{-1}. The characteristic vibrational frequencies for the main functional groups, *viz*; C–H_3 (Expt.=2924 cm^{-1}; DFT =3040 cm^{-1}), C-H $_{thiophene}$ (Expt.=3418 cm^{-1}; DFT =3220 cm^{-1}), C_{sp}2-H (Expt. = 3045 cm^{-1}; DFT =3120 cm^{-1}), C=C (Expt. = 1409 cm^{-1} ; DFT = 1467 cm^{-1}) and C=O (Expt. = 1639 cm^{-1} ; DFT = 1710 cm^{-1}). The experimental UV-visible spectrum was performed in the solvent methanol and the maximum absorption (λ_{max}) was found to be 416 nm. The FT-IR and UV-visible spectra of the chalcone compound is shown in supplementary Fig. S1 and S2.

^{1}H NMR and ^{13}C NMR spectra of 1-(5-bromothiophen-2-yl)-3-(10-chloroanthracen-9-yl)prop-2-en-1-one (3) in $CDCl_3$ shows the proposed structural formula as shown in Scheme 1. Several peaks in the aromatic region from δ 7.30 to δ 8.77 ppm were attributed to the anthracene and thiophene rings. The ^{1}H NMR of the novel chalcones suggested two doublets, one at a range of δ 8.73–8.77 ppm (for H_β) and another at a range of δ 7.15–7.16 ppm (for Hα) for vinylic protons near the carbonyl group (-CH_β=CH_α-C=O) (Fig. S3). The coupling constants value (J) ($J_{H\alpha\ -H\beta}$) for individual isomers were found to be $J_{H\alpha\ -H\beta}$ =10.7 Hz and $J_{H\alpha\ -H\beta}$ =15.6 Hz, respectively that confirms the *Cis* and *Trans* configuration of the vinylic system. ^{13}C NMR spectrum of the title compound (3) in $CDCl_3$ shows the respective peaks of carbonyl carbon (-C=O) at δ 181.00 ppm, the α, β-unsaturated carbon atoms (-CH_β=CH_α-C=O) with respect to the carbonyl carbon gives characteristic signals at δ 121.49 ppm, and 145.59 ppm respectively. The other peaks in the aromatic region from δ 122-159 ppm were attributed to the aromatic carbons of anthracene and thiophene rings as shown in Fig. S4.

Experimental mass spectra (Fig. S5) of the title compound showed the presence of molecular ion peaks $(M+H)^+$, $(M+2)^+$, and $(M+Na)^+$, corresponding to the molecular weight of chalcone derivative, one at m/z= 426.955, 428.953 and 448.936 respectively and a base peak was observed at m/z= 432.937. Due to the presence of isotopic effects of chlorine (Cl^-), bromine (Br^-), carbon and hydrogen, many peaks are observed (<0.01%) beyond the parent peak and the peaks were shown in the Table. S1.

3.3. Single crystal X-ray diffraction analysis

Single crystals of novel chalcone derivative were obtained by slow evaporation method and their molecular structures were confirmed by the X-ray diffraction analysis. The key feature of this study is that the keto-ethene group of the novel chalcone based structure exists in both *cis* and *trans* isomeric forms. Crystal form I crystallizing in monoclinic system with space group $P2_1/c$ shows *cis* configuration, while form II crystallizes in orthorhombic system with space group $P2_12_12_1$ exhibits t*rans* configuration. Fig. 3 represents the ORTEP view of the two conformers with thermal ellipsoids drawn at 50% probability. The *cis* and *trans* isomers consist keto-ethene group that connects the thiophene ring and an anthracene ring through a non-planar chain. In *cis* isomer, the thiophene ring (S1/C2/C3/C4/C5) is rotated by 21.53º from the keto-ethene group about C5-C7 bond, whereas, the connecting keto-ethene group and anthracene ring (C11-C24) are 64.57º apart indicating that the keto-ethene group is near to the thiophene ring plane. The dihedral angle between the thiophene and anthracene ring planes is 65.27º. In *trans* isomer, the thiophene ring and anthracene rings are rotated by 9.79º and 73.17º from the bridging keto-ethene group about the C5-C7 and C10-C11 respectively, indicating that the keto-ethene group is nearly coplanar to the plane of thiophene ring. The dihedral angle between the thiophene and anthracene ring planes is 82.64º. Near trigonal geometry about C7 atom is observed in both the forms that was indicated by bond angle values of C5-C7-O8 [119.77° and 119.16º], O8-C7-C9 [122.61° and 122.06º] and C5-C7-C9 [117.63° and 118.74º] in *cis* and *trans* respectively. The molecular overlay of the *cis* and *trans* conformers is shown in Fig. 2 in which the differences in molecular geometry and supramolecular recognition modes is observed. The torsion angles of the keto-ethene group is compared with the *cis* and *trans* configuration of related chalcone derivative (Table 2), 3-(9-anthryl)-1-phenylprop-2-en-1-one reported by *Ruimin Zhang et al* [59].

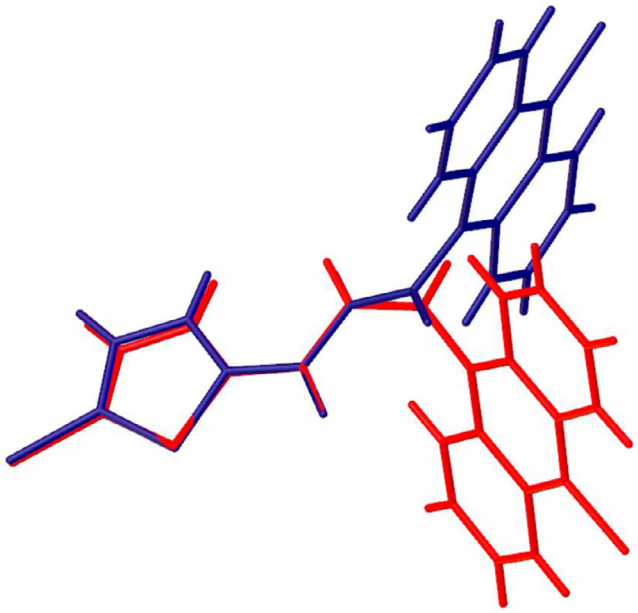

Fig. 2. Molecular overlay of cis (orange) and trans (blue) conformers.

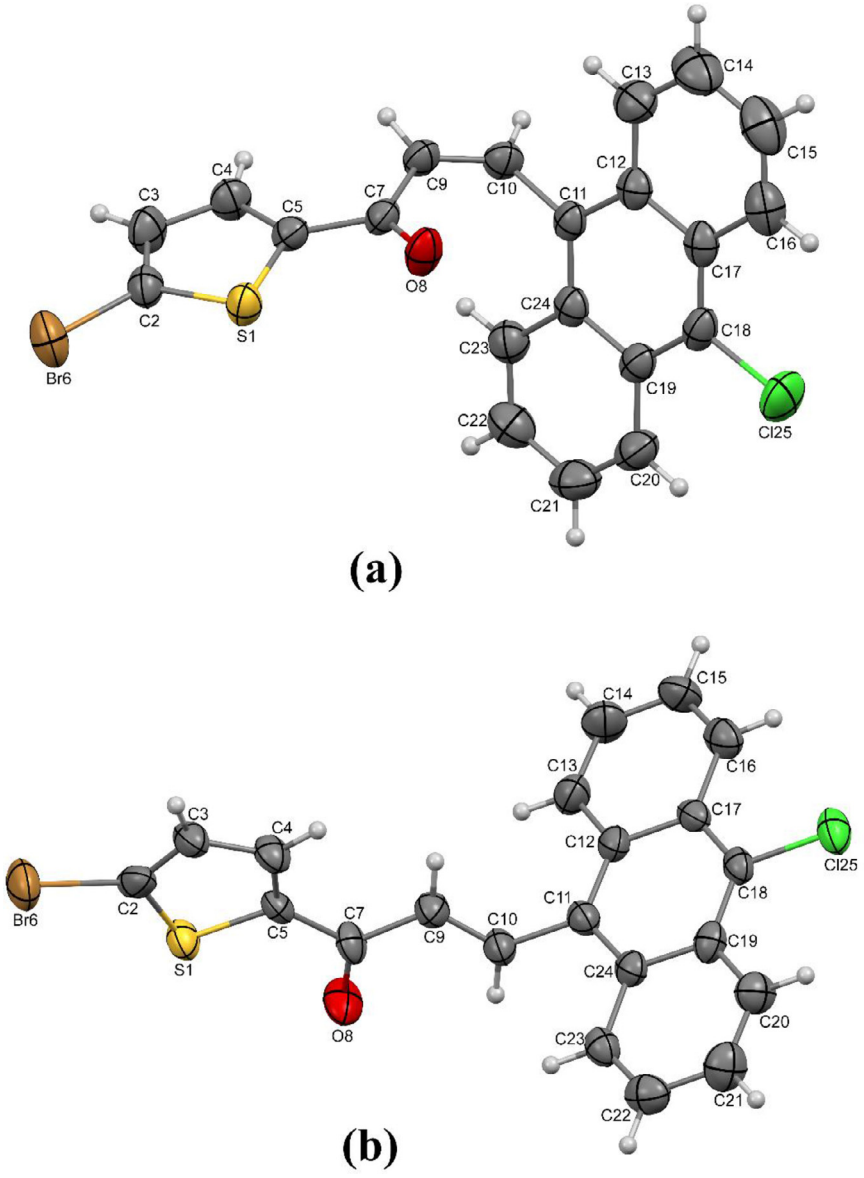

Fig. 3. ORTEP of the cis (a) and trans (b) isomer with the numbering scheme for non-hydrogen atoms and thermal ellipsoids drawn at 50% probability.

Table 2
Comparison of torsion angles (º) of the keto-ethene group in selected chalcone molecules.

C24-C11-C10-C9	C12-C11-C10-C9	C7-C9-C10-C11	O8-C7-C9-C10	C10-C9-C7-C5	C9-C7-C5-C4	
72.6(3)	-110.3(3)	1.0(4)	25.2(4)	-154.3(2)	-4.4(4)	*cis*
115.5(10)	-64.4(13)	-177.7(8)	-9.0(15)	168.5(8)	-10.8(14)	trans
-98.5(5)	82.9(5)	3.6(6)	13.1(6)	-167.4(3)	24.4(5)	*cis*[*]
97.7(5)	-80.7(5)	179.4(3)	-13.1(6)	167.1(4)	-18.0(5)	trans[*]

[*] 3-(9-anthryl)-1-phenylprop-2-en-1-one

Intramolecular C-H…Cl and dihydrogen (H…H) interaction forms two supramolecular *S(5)* and one *S(6)* pseudo rings in both the forms, however one C-H…O interaction by the keto oxygen with the ethene H10 results in the formation of *S(5)* ring only in *trans* configuration (Fig. 4). The *cis* and *trans* isomers of the chalcone derivative were stabilized by different type of non-covalent interactions (Table 3). In *cis* form, keto oxygen (O8) acts as an acceptor for two hydrogen bonding interactions (C4-H4…O8 and C9-H9…O8) forms the $R_2^1(7)$ synthon to construct 1-D zig-zig chain along crystallographic *a*-axis (Fig. 5a). S…S short contacts between the two thiophene rings interconnects the 1-D chain to generate 2-D supramolecular architecture as shown in Fig. 5b. The Cg(1)-Cg(3) interaction (Cg(1):S1/C2/C3/C4/C5 and Cg(3):C19/C20/C21/C22/C23/C24) and C-H…Cg interactions (C…Cg=3.7870(15) Å, H-Cg distance of 2.79 Å) also helps to stabilize the crystal packing. In *trans* form, strong C9-H9…O8 hydrogen bond forms an infinite 1-D linear chain along the *a*-axis $R_3^3(28)$ Thering motif rendered through C16-H16…Cl25 interconnects the 1D linear chain. Further, Br…π supramolecular interactions [Br2…π (C23 and C24)] contribute to the construction of the 3-D supramolecular architecture (Fig. 6) [60,61].

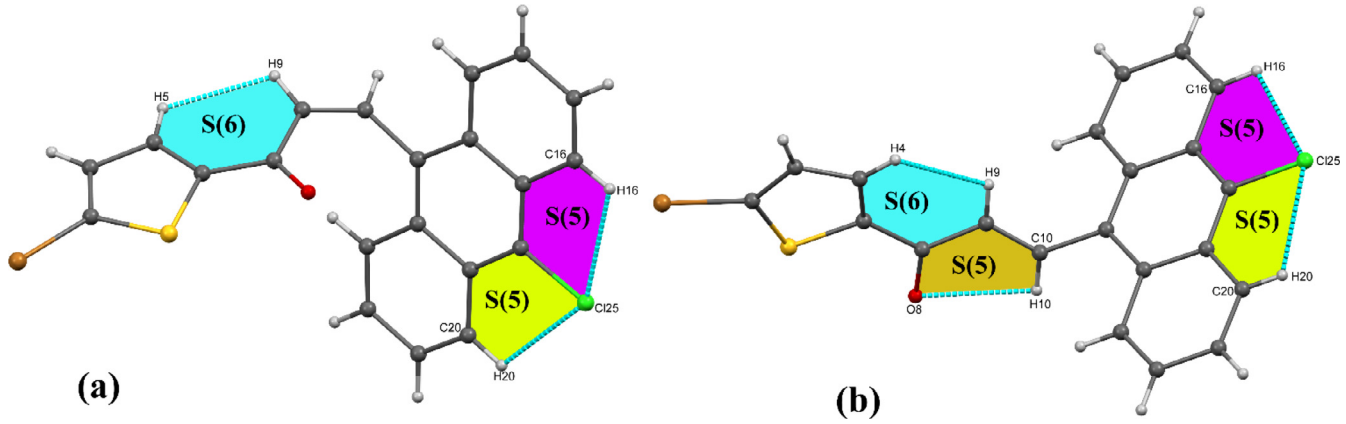

Fig. 4. *S(5)* and *S(6)* supramolecular rings formed by hydrogen bonding interactions in (a) *cis* and (b) *trans* isomers.

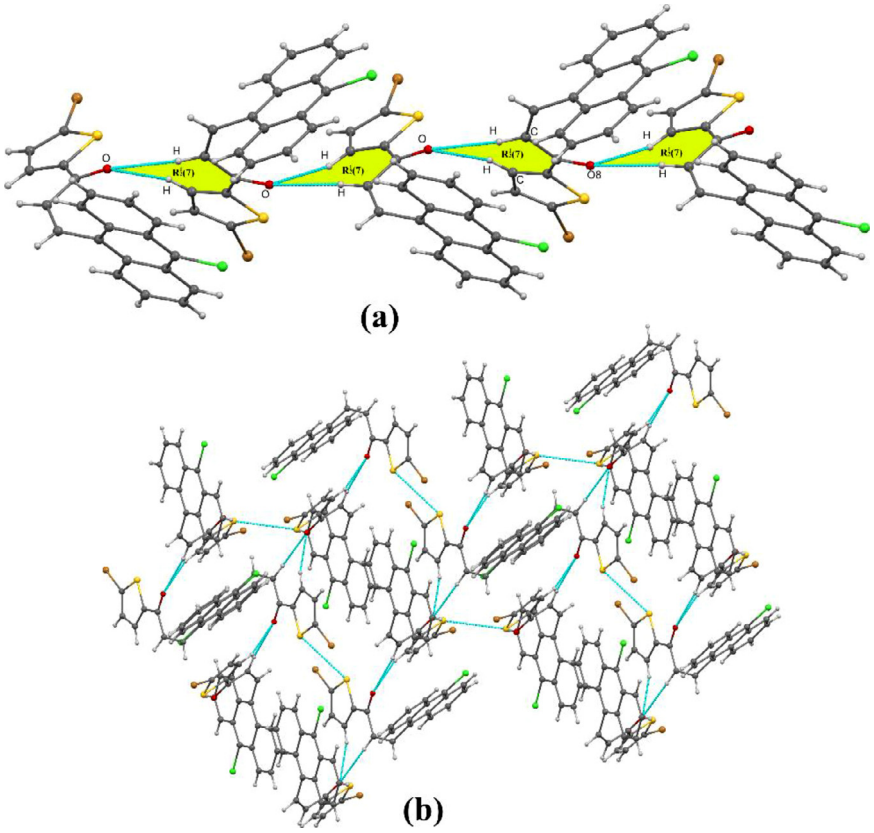

Fig. 5. (a) An infinite one-dimensional chain formed by C-H…O interactions with ring motif of $R_2^1(7)$. (b) 2-D packing arrangement in the crystal structure of *cis* isomer.

3.4. Theoretical studies

3.4.1. Hirshfeld surface analysis

The Hirshfeld surface analysis helps to explore the intermolecular interactions in crystal as they provide a visual picture of molecular shape in a crystalline environment. Intermolecular interactions of the *cis* and *trans* isomers were quantified by Hirshfeld surface analysis and their subsequent 2D fingerprint plots were explored using CrystalExplorer17 software [62]. d_{norm} surfaces were generated for *cis* and *trans* to understand the intermolecular interactions based on the crystal packing. Two wider red spots on the d_{norm} surface of the *cis* and *trans* indicates the respective acceptor and donor atoms corresponding to the strong C4-H4...O8 and C21-H21...O8 intermolecular hydrogen bond interactions (Fig. 7). Relatively smaller red dots on the d_{norm} surface of the *cis* are corresponds to the O...H and Br...H short interactions, whereas three smaller spots on d_{norm} surface of *trans* isomer indicates the Br...π short interactions and C-H...π inter contacts.

To quantify the intermolecular interactions, 2D fingerprint plots (FP) for *cis* and *trans* isomers were plotted with the range from 0.1 to 2.8 Å in each of d_i and d_e. To highlight each individual type of interactions, FPs were restrained into specific pairs of atom-types contributions (H...H, H...C, H...O, H…S and H...Br). Fig. 9 shows the 2D fingerprint plots mapped with significant intermolecular interactions, where the H...H and C...H interactions in *cis* and *trans* contribute largest to the total Hirshfeld surface with27.31% and 30.4% respectively. Two sharp spikes [d_e+d_i ~1.25 Å (*cis*) and 1.39 (*trans*) Å], indicative of a strong intermolecular hydrogen bond interaction on the fingerprint plot were observed for the O…H contacts, corresponding to the C4-H4...O8 interactions. In the vicinity of d_e+d_i

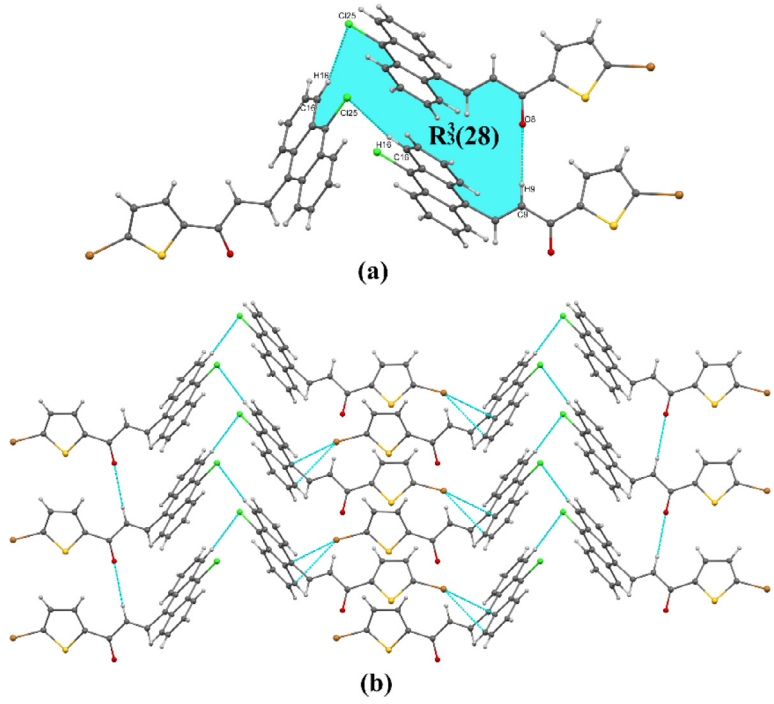

Fig. 6. $R_3^3(28)$ (a) supramolecular synthon formed by C-H…O and C-H…Cl interactions (b) 2-D zig-zag packing arrangement of the *trans* isomer.

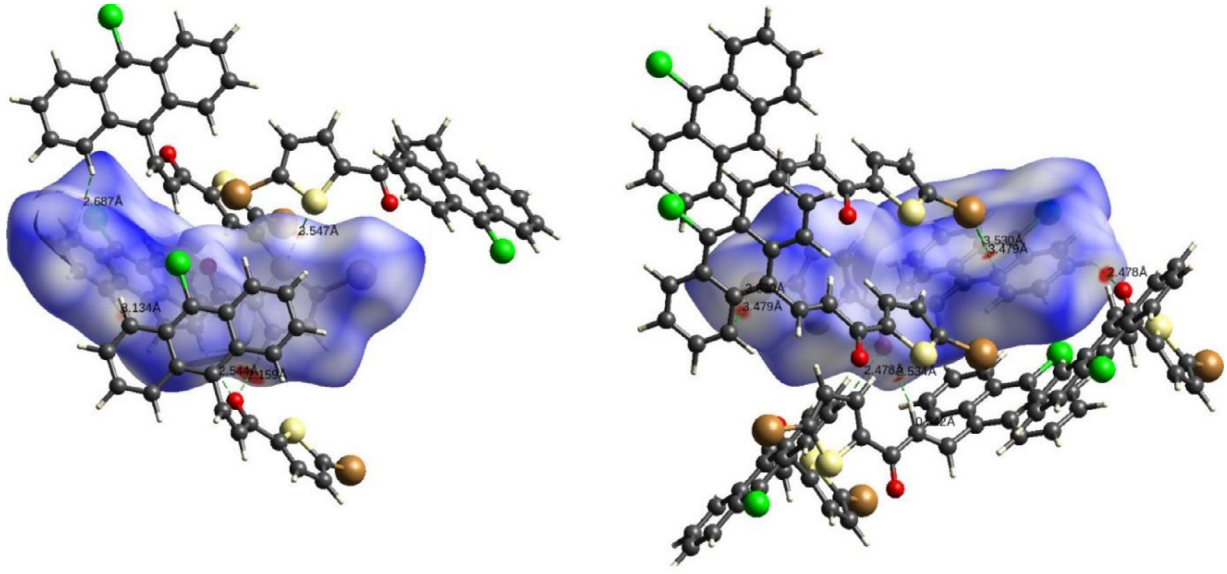

Fig. 7. d_{norm} mapped Hirshfeld surface of the *cis* (a) and *trans* (b) isomers.

Table 3
Details of hydrogen bonding interactions.

cis	D-H…A (Å)	D-H (Å)	H…A (Å)	D…A (Å)	D-H…A (°)
	C20-H20…Cl25*	0.93	2.63	3.029(3)	107
	C16-H16…Cl25*	0.93	2.64	3.035(3)	106
	C4-H4…O8^{i}	0.93	2.30	3.202(3)	162
	C9-H9…O8^{i}	0.93	2.69	3.599	165
trans	C10-H10…O8*	0.93	2.52	2.829(10)	100
	C16-H16…Cl25*	0.93	2.62	3.023(9)	107
	C20-H20…Cl25*	0.93	2.65	3.047(9)	107
	C21-H21…O8^{ii}	0.93	2.58	3.308(12)	135
	C16-H16…Cl25^{iii}	0.93	2.94	3.624	131

* intra, (i) *x*,1/2-*y*,-1/2+*z* (ii) 2-*x*,-1/2+*y*,3/2-*z* (iii) -1/2+*x*,1/2-*y*,2-*z*

~1.9 Å, another two sharp spikes are appeared for the Br…H contacts, corresponding to Br…H and Br…π short interactions for *cis* and *trans* with a contribution of 12.9% and 13.5% respectively. Apart from these major interactions, other interactions contribute considerably to the total Hirshfeld surface of *cis* and *trans* isomer (Fig. 8a).

3.4.2. Molecular interaction energy framework calculations

Energy frameworks are a convenient approach for visualizing the nature and strength of molecular interaction in crystalline materials and has been applied to understand the supramolecular organization and material level functional performance of the compounds. The interaction energy between the molecular pairs of *cis* (Table 4a) and *trans* (Table 4b) isomers were calculated for

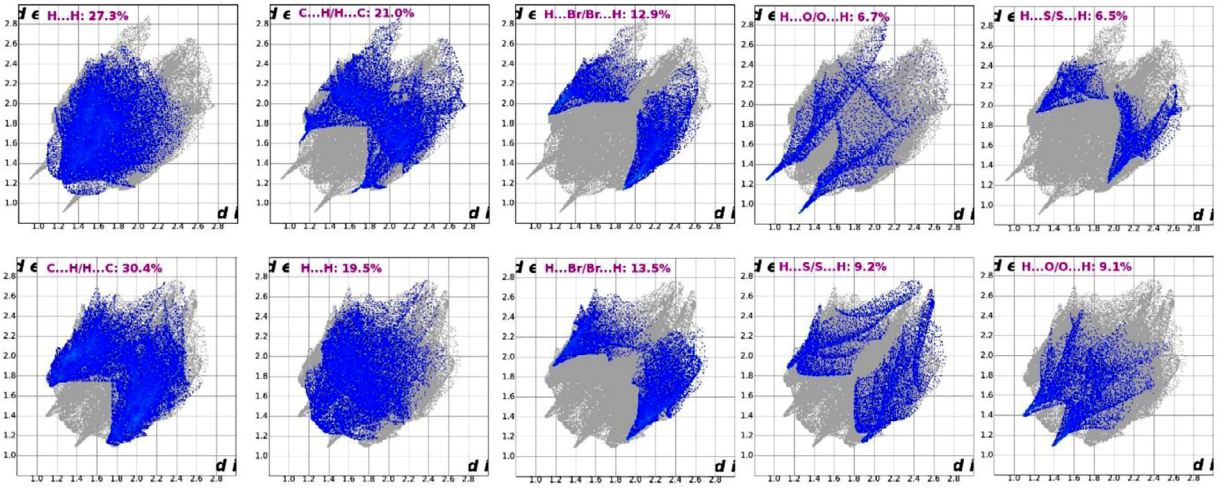

Fig. 8. 2D fingerprint plots of *cis* and *trans* isomers to represent the % contribution of various interactions to the total Hirshfeld surface.

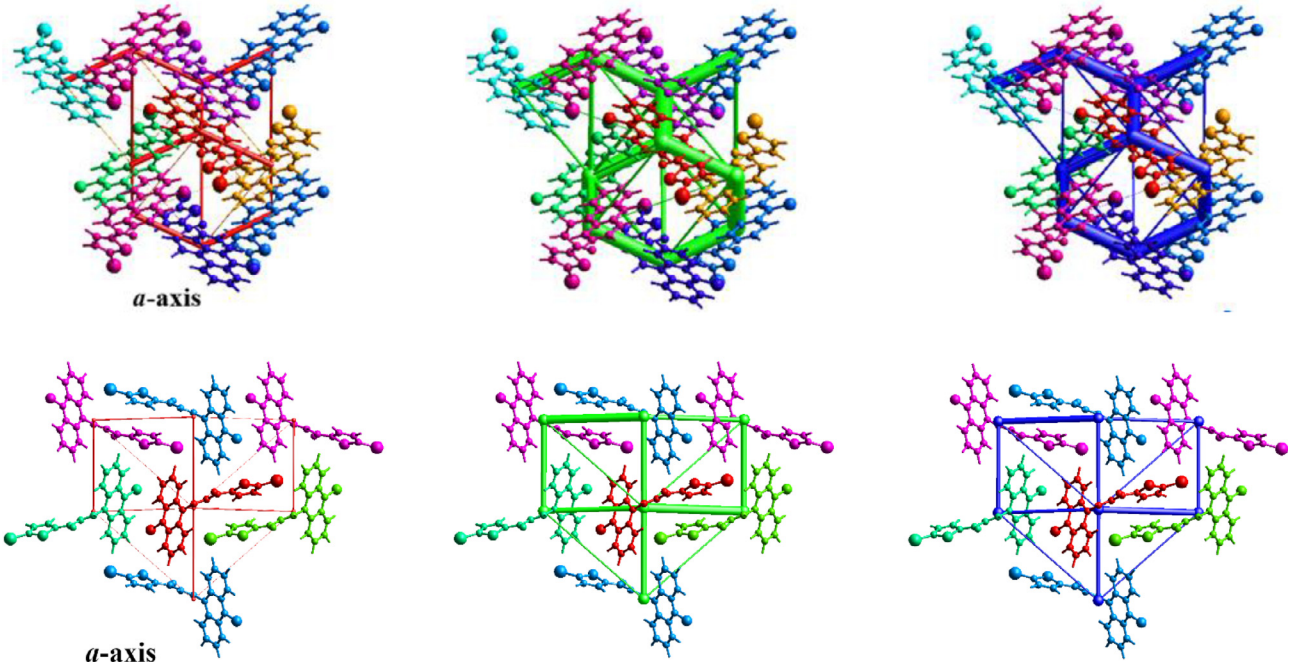

Fig. 9. Energy-frameworks for E_{ele} (red), E_{dis} (green) and E_{tot} (blue) for a cluster of fragments of (a) *cis* and (b) *trans* isomers (3.8 Å) . All diagrams use the same cylinder scale of 100 for energies.

Table 4
Molecular pairs and the interaction energies (kJ/mol) obtained from energy framework calculation for (a) ***cis*** **and (b)** ***trans*** **isomers**. R is the distance between molecular centroids in Å.

4a	N	Symop	R	E_{ele}	E_{pol}	E_{dis}	E_{rep}	E_{tot}
	2	x, y, z	12.39	-1.8	-0.4	-7.5	4.1	-5.4
	2	x, -y+1/2, z+1/2	14.12	-0.2	-0.5	-10.2	5.4	-5.3
	1	-*x*, -*y*, -*z*	9.33	-9.4	-6.5	-78.5	35.9	-55.4
	2	-*x*, *y*+1/2, -*z*+1/2	11.63	3.0	-1.0	-10	1.9	-5.1
	2	*x*, -*y*+1/2, *z*+1/2	5.59	-24.3	-9.7	-64	37.5	-58.4
	1	-*x*, -*y*, -*z*	14.89	1.0	-0.1	-4.9	2.9	-1.2
	2	-*x*, *y*+1/2, -*z*+1/2	10.19	-1.4	-1.0	-16.6	6.6	-11.7
	1	-*x*, -*y*, -*z*	8.87	-10.2	-1.9	-21.4	26.5	-9.4
	1	-*x*, -*y*, -*z*	7.36	-3.3	-2.1	-31.9	13	-23
	2	-*x*, *y*+1/2, -*z*+1/2	9.38	-3.7	-0.6	-11.2	5.8	-9.5
4b	N	Symop	R	E_{ele}	E_{pol}	E_{dis}	E_{rep}	E_{tot}
	2	*x*, *y*, *z*	5.62	-19.9	-5.7	-61.6	34	-52
	2	-*x*+1/2, -*y*, *z*+1/2	12.26	-1.4	-0.4	-9.3	2.6	-7.9
	2	*x*+1/2, -*y*+1/2, -*z*	7.19	-5.7	-2.8	-45.6	22.8	-30.2
	2	*x*+1/2, -*y*+1/2, -*z*	12.41	-2.8	-1.2	-27.4	15.2	-16
	2	-*x*, *y*+1/2, -*z*+1/2	10.10	-7.3	-2.3	-10.5	5.4	-14
	2	-*x*, *y*+1/2, -*z*+1/2	8.91	-2.4	-1.5	-29.4	14.7	-18
	2	-*x*+1/2, -*y*, *z*+1/2	11.89	-1	-0.3	-8.8	3.3	-6.4

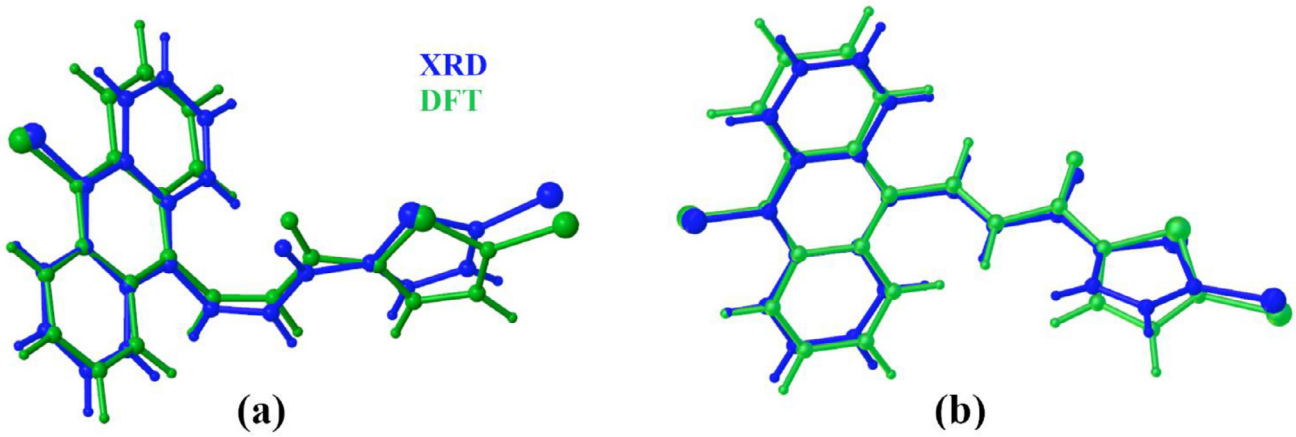

Fig. 10. Overlay of the crystal structure and optimized structure of (a) *cis* and (b) *trans* isomers of chalcone derivative.

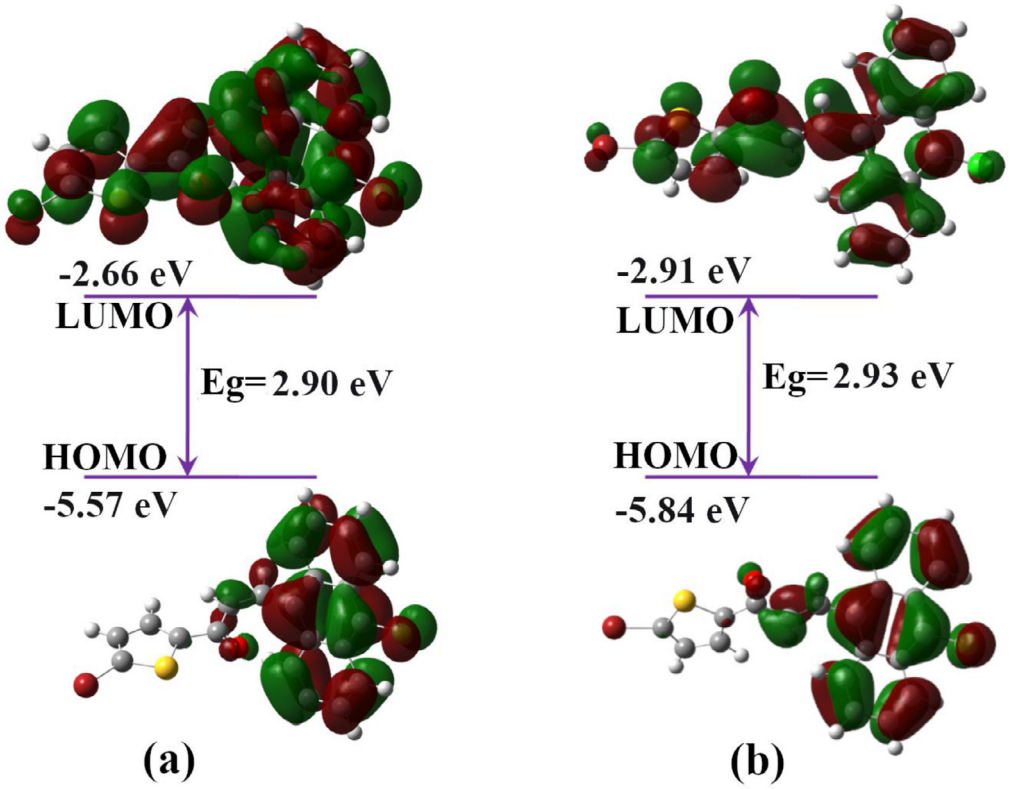

Fig. 11. Frontier molecular orbital profile of the (a) *cis* and (b) *trans* isomers of chalcone derivative.

the construction of energy frameworks to evaluate the net interaction energy. The variation in the crystal packing modes and true synthon hierarchy of the isomeric crystal structures were investigated. A systematic comparison of the electrostatic, dispersion and total energy frameworks of the two isomers shows the dissimilarities in their energy frameworks (Fig. 9). A variation in the dimensions of the pillars, columns and crossbars between the two forms are observed. The energy frameworks of *cis* form view along the *a*-axis is shown in Fig. 10a. The pyramid-like packing arrangement in *cis* is observed with dominant dispersion energy component. The total energy of the molecular fragments (E_{tot}=-184.4 kJ/mol) comprises of electrostatic (E_{ele}=-51.25 kJ/mol), polarization (E_{pol}=-15.49 kJ/mol), dispersion (E_{dis}=-230.74 kJ/mol) and exchange-repulsion (Erep = 113.21 kJ/mol) energies. In *trans* isomer, interconnected square type topologies around the central molecule is observed (Fig.) with the various interaction energies, E_{ele} = -41.26 kJ/mol, E_{pol}= -9.242 kJ/mol, E_{dis} = -173.53 kJ/mol, E_{rep} = 79.47 kJ/mol and E_{tot} = -144.56 kJ/mol. The frameworks analysis enlightens the relatively more anisotropic nature in the packing of *cis* compared to *trans* isomer [63].

3.4.3. Density functional theory (DFT) calculations

Cis and *trans* isomers were optimized using DFT calculations to explore the geometric parameters, bond lengths, bond angles and torsional angles. A very good agreement is observed between the single crystal X-ray diffraction (XRD) and the optimized geometrical parameters. The bond lengths, bond angles and torsional angles (XRD and DFT) and their correlation coefficients are listed in Tables S2 and S3. An overlay of the crystal structure and optimized electronic structure is displayed in Fig. 10. Root mean square deviations (RMSDs) of 0.406 Å and 0.475 Å are observed for *cis* and *trans* isomers respectively. The ground state energies of the opti-

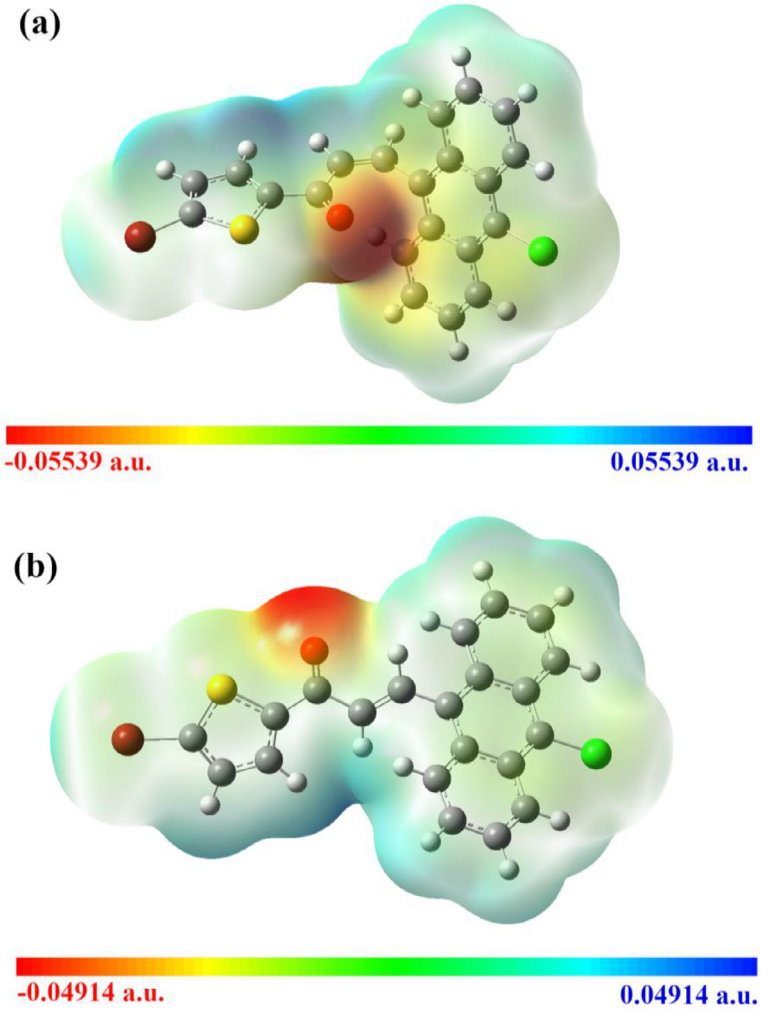

Fig. 12. Molecular electrostatic potential map of the (a) *cis*, and (b) *trans* isomers of chalcone derivative.

mized structures are 4315.46 and 4312.19 Hartree for *cis* and *trans* isomers respectively. Kohn-Sham frontier molecular orbital calculations were performed to understand the electronic, electrochemical and optical properties of the novel chalcone derivative. The 3-D plots of the highest occupied molecular orbital (HOMO) and lowest unoccupied molecular orbital (LUMO) of the *cis* and *trans* isomers (red and green colours represent the positive and negative regions) with the isovalue of 0.02 are shown in Fig. 11. Molecular orbital profile revealed that the localization of HOMO is majorly occurred around anthracene ring in both the forms, whereas LUMO is mainly localized about both anthracene and thiophene rings. The HOMO and LUMO molecular orbital energy for *cis*/*trans* forms are -5.5666/-5.8360 eV and -2.6646/-2.9094 eV, respectively. The FMOs play a significant role in the intermolecular charge transfer from donor to acceptor moiety of the molecular system that helps to understand the chemical reactive parameters of the molecule. The calculated HOMO-LUMO energy gap is 2.9019 and 2.9266 eV for *cis* and *trans* isomers respectively, and it is a key stability index for the chemical reactive parameters. The ionization potential ($I = -E_{HOMO}$), the electron affinity ($A = -E_{LUMO}$), the absolute electronegativity (χ), the global hardness (η), global softness (σ), the global electrophilicity (ω), the chemical potential ($\mu = -\chi$) and the electronic dipole moment (Debye) were calculated and are listed in Table 5. [64–67]. In the intermolecular charge transfer process HOMO and LUMO are the first orbitals to donate and accept the electrons in the molecular system which highlights the reactivity of the compound. The binding ability of the molecule is increases with increasing in HOMO and decreasing in LUMO energy values. The smaller HOMO-LUMO energy gap indicates the softness of the molecule with more reactivity and less stability. Electrophilicity index is a measure of propensity of a chemical species to accept electrons and the more stable molecule corresponds to lesser electrophilicity and vice versa.

Table 5
Global and local parameters of the *cis* and *trans* isomers.

Parameters	*cis*	*trans*
E_{HOMO}	-5.57 eV	-5.84 eV
E_{LUMO}	-2.66 eV	-2.91 eV
ΔE_{gap}	2.90 eV	2.93 eV
Ionization potential (I)	5.57 eV	5.84 eV
Electron affinity (A)	2.66 eV	2.91 eV
Electronegativity (χ)	4.12 eV	4.37 eV
Global hardness (η)	1.45 eV	1.46 eV
Global softness (σ)	0.69 eV^{-1}	0.68 eV^{-1}
Electrophilicity (ω)	12.29 eV	6.53 eV
Chemical potential(μ)	-4.12 eV	-4.37 eV
Dipole moment	4.66 Debye	2.67 Debye

Where, $\chi = (I+A)/2$, $\eta = (I-A)/2$, $\sigma = 1/\eta$ and $\omega = \mu^2/2$

The three dimensional molecular electrostatic potential (MEP) analysis can be used to identify the possible chemically reactive sites of a system by predicting electrophilic (blue) and nucleophilic

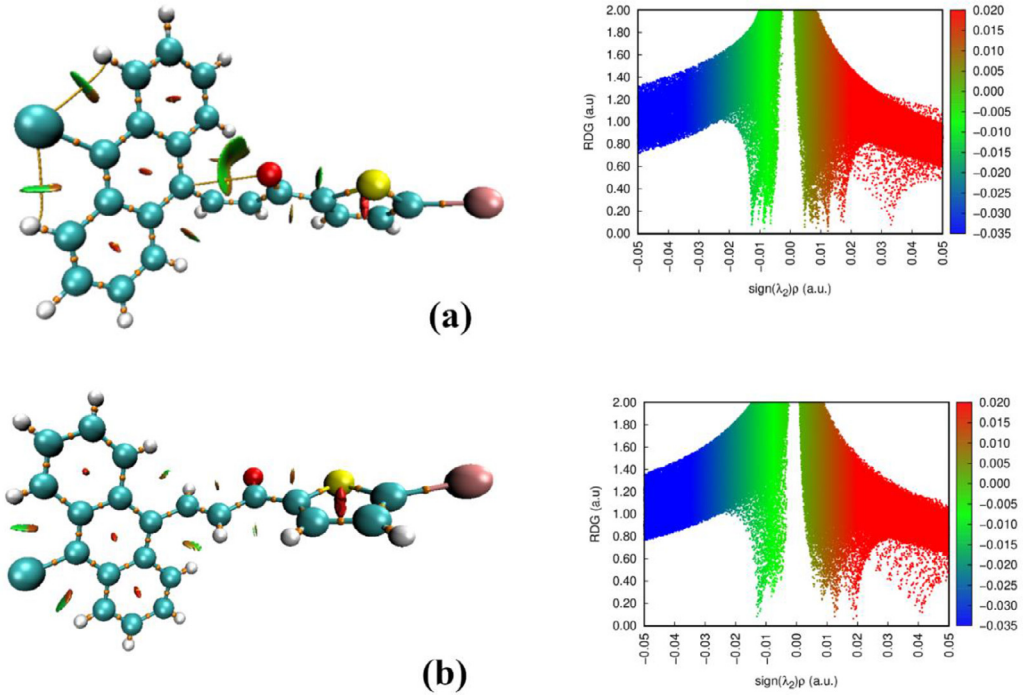

Fig. 13. 3D non-covalent interactions and 2D scatter plot of *cis* (a) and *trans* (b) isomers with an isosurface value of 0.5.

(red) sites. MEP with color scale representing the charge distribution of molecule. The difference in colour variation on the molecular surface will helps to identify the chemically active regions of the molecule (Fig. 13). In both the forms (*cis* and *trans*) negatively active region (red) is majorly distributed on oxygen atom (O8) in the molecular surface with the maximum values of -0.0545 (*cis*) and -0.0488 (*trans*) supports to the electrophilic attack. However, smaller electrophilic nature on Br6 and S1 of bromothiophene is indicated by orange and yellow colored region. The blue regions are largely localized on the hydrogen atom H4 (0.0349) and H9 (0.0417) shows the participation of hydrogen atoms in significant (C-H…O) interactions in both *cis* and *trans* isomers (Fig. 12).

3.4.4. QTAIM and NCI index analysis

The strength and nature of intramolecular interactions can be identified and analysed based on the electron density distribution in the molecule. The critical points and bond paths in the Bader's QTAIM framework reveal the presence of various non-covalent interactions. The reduced density gradient based NCI indexed model for the *cis* and *trans* isomers are shown in Fig. 13 with isosurface value 0.05. NCI model shows that both the conformers have similar type of major intramolecular interactions C16-H16…Cl25, C20-H20…Cl25, C10-H10…O8 and dihydrogen (H4…H9) but the strength of the interactions are different. In both the forms, the red coloured disks in the middle of all the four rings indicate the ring-strain, and the major steric repulsion is observed due to the thiophene ring. 2D scatter plot derived from the electron density of the respective molecule to elucidate strength and nature of various intramolecular interaction. The low-gradient spike with the low density lying at negative values indicates the attractive non-covalent interactions and the red coloured spike near 0.03-0.4 a.u. shows the repulsive interaction [68].

4. Conclusions

In summary, we have successfully synthesized a novel chalcone derivative and the crystal structure analysis revealed the *cis* and *trans* isomerism. The specific molecular conformation and crystal packing modes are analyzed by X-ray diffraction analysis and the configuration of the isomers display significant deviations from planarity. The dihedral angle between the thiophene and anthracene ring planes are 65.27º (*cis*) and 82.64º (*trans*) indicates a significant twist in both the forms. C-H…O, S…S and C-H…π contacts in *cis*, and C-H…O, C-H…Cl, and Br…π intermolecular interactions in *trans* provide a stabilized molecular packing. These interactions lead to the construction of unique and different aesthetic supramolecular framework in two isomers. The differences and similarities in the packing mode of isomeric crystal structures (*cis* and *trans*) are revealed by Hirshfeld surface and energy framework analysis. The frontier molecular orbital energies were calculated and the HOMO-LUMO energy gap of *cis* and *trans* isomer was found to be 2.9019 and 2.9266 eV respectively. The nucleophilic and electrophilic regions of the molecule on the molecular surface were identified using MEP.

Authors' contribution

All authors contributed to discussions and preparation of the manuscript.

NKL, SN, PN and PB designed the work and performed the single crystal X-ray diffraction experiment and theoretical calculations.

PN, SG, JP and KS performed the synthesis and spectroscopic characterizations.

WM and SN performed Hirshfeld Surface Analysis.

Authorship statement

All persons who meet authorship criteria are listed as authors, and all authors certify that they have participated sufficiently in the work to take public responsibility for the content, including participation in the concept, design, analysis, writing, or revision of the manuscript. Furthermore, each author certifies that this material or similar material has not been and will not be submitted to or published in any other publication before its appearance in the Journal of Molecular Structure Authorship contribu-

tions Please indicate the specific contributions made by each author (list the authors' initials followed by their surnames, The name of each author must appear at least once in each of the three categories below. Category 1 Conception and design of study: Naresh P., Pramod B., Naveen S., Ganguly S., Panda J., Sunitha K., Maniukiewicz W and Lokanath N. K. Acquisition of data: Naresh P, Naveen S., Neratur Krishnappagowda Lokanath Analysis and/or interpretation of data: Naveen S., Pramodh B., Ganguly P., Neratur Krishnappagowda Lokanath Category 2 Drafting the manuscript: Naresh P., Naveen S., Sunitha K., Maniukiewicz W., Panda J., Neratur Krishnappagowda Lokanath Revising the manuscript critically for important intellectual content: Naresh P., Naveen S., Pramodh B., Neratur Krishnappagowda Lokanath Category 3 Approval of the version of the manuscript to be published (the names of all authors must be listed): Naresh P., Pramod B., Naveen S., Ganguly S., Panda J., Sunitha K., Maniukiewicz W and Lokanath N. K. Acknowledgements All persons who have made substantial contributions to the work reported in the manuscript (e.g., technical help, writing and editing assistance, general support), but who do not meet the criteria for authorship, are named in the Acknowledgements and have given us their written permission to be named. If we have not included an Acknowledgements, then that indicates that we have not received substantial contributions from non-authors.

Declaration of Competing Interest

The authors declare that they have no known competing financial interests or personal relationships that could have appeared to influence the work reported in this paper.

Acknowledgments

The authors are grateful to the National Single Crystal Diffractometer Facility, Department of Studies in Physics, University of Mysore, Manasagangotri, Mysuru for providing the X-ray intensity data. The authors acknowledge the financial support of UGC-IOE and DST -PURSE projects. The authors also thank Prof. D. B. Ramachary, School of Chemistry, University of Hyderabad for the help in crystallization of the title compound.

Supplementary materials

Supplementary material associated with this article can be found, in the online version, at doi:10.1016/j.molstruc.2021.130228.

References

[1] D.K. Mahapatra, S.K. Bharti, V. Asati, Chalcone scaffolds as anti-infective agents: structural and molecular target perspectives, Eur. J. Med. Chem. 101 (2015) 496–524, doi:10.1016/j.ejmech.2015.06.052.
[2] D.K. Mahapatra, S.K. Bharti, V. Asati, Anti-cancer chalcones: structural and molecular target perspectives, Eur. J. Med. Chem. 98 (2015) 69–114, doi:10.1016/j.ejmech.2015.05.004.
[3] D.K. Mahapatra, V. Asati, S.K. Bharti, Chalcones and their therapeutic targets for the management of diabetes: structural and pharmacological perspectives, Eur. J. Med. Chem. 92 (2015) 839–865, doi:10.1016/j.ejmech.2015.01.051.
[4] S. Alen, D. Sajan, L. Joseph, K. Chaitanya, V. Shettigar, V.B. Jothy, Synthesis, growth, vibrational spectral investigations and structure-property relationship of an organic NLO crystal: 3,4-dimethoxy chalcone, Chem. Phys. Lett. 636 (2015) 208–215, doi:10.1016/j.cplett.2015.07.030.
[5] S. Gronowitz, *Thiophene and its Derivatives, Part 4* (Vol. 152), John Wiley and Sons, 2009.
[6] M.S. Yen, I.J. Wang, Synthesis and absorption spectra of hetarylazo dyes derived from coupler 4-aryl-3-cyano-2-aminothiophenes, Dye. Pigment. 61 (2004) 243–250, doi:10.1016/j.dyepig.2003.10.015.
[7] D.M. Vriezema, J. Hoogboom, K. Velonia, K. Takazawa, P.C.M. Christianen, J.C. Maan, A.E. Rowan, R.J. Nolte, Vesicles and polymerized vesicles from thiophene-containing rod–coil block copolymers, Angew. Chemie 42 (7) (2003) 772–776, doi:10.1002/anie.200390204.
[8] H.H. Yu, A.E. Pullen, M.G. Büschel, T.M. Swager, Charge-specific interactions in segmented conducting polymers: an approach to selective ionoresistive responses, Angew. Chemie - Int. Ed. 43 (28) (2004) 3700–3703, doi:10.1002/anie.200453896.
[9] M. Halik, H. Klauk, U. Zschieschang, G. Schmid, S. Ponomarenko, S. Kirchmeyer, W. Weber, Relationship between molecular structure and electrical performance of oligothiophene organic thin film transistors, Adv. Mater. 15 (11) (2003) 917–922, doi:10.1002/adma.200304654.
[10] C. Rost, S. Karg, W. Riess, M.A. Loi, M. Murgia, M. Muccini, Ambipolar light-emitting organic field-effect transistor, Appl. Phys. Lett. 85 (9) (2004) 1613–1615, doi:10.1063/1.1785290.
[11] M. Benabdellah, A. Aouniti, A. Dafali, B. Hammouti, M. Benkaddour, A. Yahyi, A. Ettouhami, Investigation of the inhibitive effect of triphenyltin 2-thiophene carboxylate on corrosion of steel in 2 M H 3 PO 4 solutions, Appl. Surf. Sci. 252 (23) (2006) 8341–8347, doi:10.1016/j.apsusc.2005.11.037.
[12] H. Xu, R. Chen, Q. Sun, W. Lai, Q. Su, W. Huang, X. Liu, Recent progress in metal-organic complexes for optoelectronic applications, Chem. Soc. Rev. 43 (10) (2014) 3259–3302, doi:10.1039/c3cs60449g.
[13] G.S. He, L.S. Tan, Q. Zheng, P.N. Prasad, Multiphoton absorbing materials: molecular designs, characterizations, and applications, Chem. Rev. 108 (4) (2008) 1245–1330, doi:10.1021/cr050054x.
[14] R.D. Wampler, A.J. Moad, C.W. Moad, R. Heiland, G.J. Simpson, Visual methods for interpreting optical nonlinearity at the molecular level, Acc. Chem. Res. 40 (10) (2007) 953–960, doi:10.1021/ar600055t.
[15] X.C. Li, C.Y. Wang, W.Y. Lai, W. Huang, Triazatruxene-based materials for organic electronics and optoelectronics, J. Mater. Chem. C 4 (2016) 10574–10587, doi:10.1039/c6tc03832h.
[16] D.A. Zainuri, I.A. Razak, S. Arshad, Mol-ecular structure, DFT studies and UV-Vis absorption of two new linear fused ring chalcones: (E)-1-(anthracen-9-yl)-3-(2-meth-oxy-phen-yl)prop-2-en-1-one and (E)-1-(anthracen-9-yl)-3-(3-fluoro-4-meth-oxy-phen-yl)prop-2-en-1-one, Acta Crystallogr. Sect. E Crystallogr. Commun. 74 (2018) 1087–1092, doi:10.1107/S205698901800974X.
[17] D.A. Zainuri, I.A. Razak, S. Arshad, Crystal structure and theoretical studies of two π-conjugated fused-ring chalcones: (E)-1-(anthracen-9-yl)-3-(9-ethyl-9 H-carbazol-3-yl)prop-2-en-1-one and (E)-1-(anthracen-9-yl)-3-[4-(9 H-carbazol-9-yl)phenyl]prop-2-en-1-one, Acta Crystallogr. Sect. E Crystallogr. Commun. 74 (2018) 1302–1308, doi:10.1107/S2056989018011131.
[18] Di.A. Zainuri, I.A. Razak, S. Arshad, Crystal structure, spectroscopic characterization and DFT study of two new linear fused-ring chalcones, Acta Crystallogr. Sect. E Crystallogr. Commun. 74 (2018) 1427–1432, doi:10.1107/S2056989018012641.
[19] D.A. Zainuri, I.A. Razak, S. Arshad, Molecular structure, DFT studies and Hirshfeld analysis of anthracenyl chalcone derivatives, Acta Crystallogr. Sect. E Crystallogr. Commun. 74 (2018) 780–785, doi:10.1107/S2056989018006527.
[20] P.S. Patil, S.R. Maidur, J.R. Jahagirdar, T.S. Chia, C.K. Quah, M. Shkir, Crystal structure, spectroscopic analyses, linear and third-order nonlinear optical properties of anthracene-based chalcone derivative for visible laser protection, Appl. Phys. B Lasers Opt. 125 (2019) 1–13, doi:10.1007/s00340-019-7275-z.
[21] M.F. Zaini, I.A. Razak, W.M. Khairul, S. Arshad, Crystal structure and optical properties of fused ring chalcone (E)-3-(anthracen-9-yl)-1-(4-nitrophenyl) prop-2-en-1-one, Acta Crystallogr. Sect. E Crystallogr. Commun. 75 (2019) 685–689, doi:10.1107/S2056989019005243.
[22] W. Zhou, Y. Fang, X. Wu, Y. Han, J. Yang, L. Shen, Y. Song, Anthracene derivatives as broadband nonlinear optical materials: nonlinear absorption and excited-state dynamics analysis, RSC Adv. 10 (2020) 19974–19981, doi:10.1039/d0ra02638g.
[23] M. Chen, L. Yan, Y. Zhao, I. Murtaza, H. Meng, W. Huang, Anthracene-based semiconductors for organic field-effect transistors, J. Mater. Chem. C 6 (2018) 7416–7444, doi:10.1039/c8tc01865k.
[24] D. Zych, A. Slodek, M. Matussek, M. Filapek, G. Szafraniec-Gorol, S. Maślanka, S. Krompiec, S. Kotowicz, E. Schab-Balcerzak, K. Smolarek, S. Maćkowski, M. Olejnik, W. Danikiewicz, 4′-Phenyl-2,2′:6′,2″-terpyridine derivatives-synthesis, potential application and the influence of acetylene linker on their properties, Dye. Pigment. 146 (2017) 331–343, doi:10.1016/j.dyepig.2017.07.030.
[25] D. Zych, A. Slodek, D. Zimny, S. Golba, K. Malarz, A. Mrozek-Wilczkiewicz, Influence of the substituent D/A at the 1,2,3-triazole ring on novel terpyridine derivatives: synthesis and properties, RSC Adv. 9 (2019) 16554–16564, doi:10.1039/c9ra02655j.
[26] D. Zych, A. Slodek, Acceptor-π-acceptor-acceptor/donor systems containing dicyanovinyl acceptor group with substituted 1,2,3-triazole motif – synthesis, photophysical and theoretical studies, J. Mol. Struct. 1204 (2020) 127488, doi:10.1016/j.molstruc.2019.127488.
[27] D.A. Zainuri, M. Abdullah, S. Arshad, M.S.A. Aziz, G. Krishnan, H. Bakhtiar, I.A. Razak, Crystal structure, spectroscopic and third-order nonlinear optical susceptibility of linear fused ring dichloro-substituent chalcone isomers, Opt. Mater. (Amst). 86 (2018) 32–45, doi:10.1016/j.optmat.2018.09.032.
[28] T. Hinoue, Y. Shigenoi, M. Sugino, Y. Mizobe, I. Hisaki, M. Miyata, N. Tohnai, Regulation of π-stacked anthracene arrangement for fluorescence modulation of organic solid from monomer to excited oligomer emission, Chem. - Eur. J. 18 (2012) 4634–4643, doi:10.1002/chem.201103518.
[29] Y. Inoue, S. Tokito, K. Ito, T. Suzuki, Organic thin-film transistors based on anthracene oligomers, J. Appl. Phys. 95 (2004) 5795–5799, doi:10.1063/1.1707206.
[30] S. Toyota, M. Yoshikawa, T. Saibara, Y. Yokoyama, T. Komori, T. Iwanaga, Chemistry of anthracene−acetylene oligomers XXVII. Iterative synthesis, structures, and properties of anthracene−diacetylene cyclic oligomers with 10-mesitylanthracene-1,8-diyl units, Chempluschem 84 (2019) 643–654, doi:10.1002/cplu.201800433.
[31] G.R. Desiraju, Crystal engineering: from molecule to crystal, J. Am. Chem. Soc. 135 (27) (2013) 9952–9967, doi:10.1021/ja403264c.

[32] M.K.Hema Mahesha, C.S. Karthik, K.J. Pampa, P. Mallu, N.K. Lokanath, Solvent induced mononuclear and dinuclear mixed ligand Cu(ii) complex: structural diversity, supramolecular packing polymorphism and molecular docking studies, New J. Chem. 44 (41) (2020) 18048–18068, doi:10.1039/d0nj03567j.
[33] Z.H. Zhu, H.L. Wang, H.H. Zou, F.P. Liang, Metal hydrogen-bonded organic frameworks: structure and performance, Dalt. Trans. 49 (31) (2020) 10708–10723, doi:10.1039/d0dt01998d.
[34] S.K. Seth, I. Saha, C. Estarellas, A. Frontera, T. Kar, S. Mukhopadhyay, Supramolecular self-assembly of M-IDA complexes involving lone-pair ···φ Interactions: crystal structures, hirshfeld surface analysis, and DFT calculations [H2IDA = iminodiacetic acid, M = Cu(II), Ni(II)], Cryst. Growth Des. 11 (7) (2011) 3250–3265, doi:10.1021/cg200506q.
[35] J. Bauer, S. Spanton, R. Henry, J. Quick, W. Dziki, W. Porter, J. Morris, Ritonavir: an extraordinary example of conformational polymorphism, Pharm. Res. 18 (6) (2001) 859–866, doi:10.1023/A:1011052932607.
[36] S. Datta, D.J.W. Grant, Crystal structures of drugs: advances in determination, prediction and engineering, Nat. Rev. Drug Discov. 3 (1) (2004) 42–57, doi:10.1038/nrd1280.
[37] L.F. Huang, W.Q. Tong, Impact of solid state properties on developability assessment of drug candidates, Adv. Drug Deliv. Rev. 56 (3) (2004) 321–334, doi:10.1016/j.addr.2003.10.007.
[38] S.L. Morissette, Ö. Almarsson, M.L. Peterson, J.F. Remenar, M.J. Read, A.V. Lemmo, S. Ellis, M.J. Cima, C.R. Gardner, High-throughput crystallization: polymorphs, salts, co-crystals and solvates of pharmaceutical solids, Adv. Drug Deliv. Rev. 56 (3) (2004) 275–300, doi:10.1016/j.addr.2003.10.020.
[39] N. Panigrahi, S. Ganguly, J. Panda, Y. Praharsha, Ultrasound assisted synthesis and antimicrobial evaluation of novel thiophene chalcone derivatives, Chem. Sci. Trans. 3 (2014) 1163–1171, doi:10.7598/cst2014.842.
[40] N. Panigrahi, S. Ganguly, J. Panda, Synthesis, antimicrobial evaluation and molecular docking studies of novel oxazolidinone-thiophene chalcone hybrid derivatives, Res. J. Pharm. Technol. 11 (2018) 5611–5622, doi:10.5958/0974-360X.2018.01019.3.
[41] Expert, C. S. (2011). Rigaku Corporation. Tokyo, Japan.
[42] G.M. Sheldrick, A short history of SHELX, Acta Crystallogr. Sect. A Found. Crystallogr. 64 (1) (2008) 112–122, doi:10.1107/S0108767307043930.
[43] G.M. Sheldrick, Crystal structure refinement with SHELXL, Acta Crystallogr. Sect. C Struct. Chem. 71 (1) (2015) 3–8, doi:10.1107/S2053229614024218.
[44] O.V. Dolomanov, L.J. Bourhis, R.J. Gildea, J.A.K. Howard, H. Puschmann, OLEX2: a complete structure solution, refinement and analysis program, J. Appl. Crystallogr. 42 (2) (2009) 339–341, doi:10.1107/S0021889808042726.
[45] C.F. MacRae, I. Sovago, S.J. Cottrell, P.T.A. Galek, P. McCabe, E. Pidcock, M. Platings, G.P. Shields, J.S. Stevens, M. Towler, P.A. Wood, Mercury 4.0: from visualization to analysis, design and prediction, J. Appl. Crystallogr. 53 (1) (2020) 226–235, doi:10.1107/S1600576719014092.
[46] M.J. Turner, J.J. McKinnon, S.K. Wolff, D.J. Grimwood, P.R. Spackman, D. Jayatilaka, M.A. Spackman, CrystalExplorer17, University of Western Australia, 2017 https://hirshfeldsurface.net.
[47] M.A. Spackman, D. Jayatilaka, Hirshfeld surface analysis, CrystEngComm 11 (1) (2009) 19–32, doi:10.1039/b818330a.
[48] H.M. Mahesha, M.K. Hema, C.S. Karthik, J.K. Pampa, P. Mallu, N.K. Lokanath, μ-phenoxide bridged mixed ligand Cu(II) complex: synthesis, 3D supramolecular architecture, DFT, energy frameworks and antimicrobial studies, Polyhedron 185 (2020) 114571, doi:10.1016/j.poly.2020.114571.
[49] P.C. Hariharan, J.A. Pople, The influence of polarization functions on molecular orbital hydrogenation energies, Theor. Chim. Acta 28 (3) (1973) 213–222, doi:10.1007/BF00533485.
[50] J.M. Seminario, Recent Developments and Applications of Modern Density Functional Theory, Elsevier, 1996.
[51] Frisch, M. J., Trucks, G. W., Schlegel, H. B., Scuseria, G. E., Robb, M. A., Cheeseman J. R., and Li, X., Gaussian 16, (2016).
[52] Dennington, R. D., Keith T. A., and Millam, J. M., GaussView 6.0.16, 2016.
[53] T. Lu, F. Chen, Multiwfn: a multifunctional wavefunction analyzer, J. Comput. Chem. 33 (5) (2012) 580–592, doi:10.1002/jcc.22885.
[54] B.Evranos Aksöz, R. Ertan, Chemical and structural properties of chalcones I, Fabad J. Pharm. Sci. 36 (2011) 223–242.
[55] M.J.G. Moa, M. Mandado, M.N.D.S. Cordeiro, R.A. Mosquera, QTAIM electron density study of natural chalcones, Chem. Phys. Lett. 446 (2007) 1–7, doi:10.1016/j.cplett.2007.08.021.
[56] M. Oumi, D. Maurice, M. Head-Gordon, Ab initio calculations of the absorption spectrum of chalcone, Spectrochim. Acta - Part A Mol. Biomol. Spectrosc. 55 (1999) 525–537, doi:10.1016/S1386-1425(98)00260-1.
[57] Y. Xue, X. Gong, The conformational, electronic and spectral properties of chalcones: a density functional theory study, J. Mol. Struct. Theochem. 901 (2009) 226–231, doi:10.1016/j.theochem.2009.01.034.
[58] D.E. Nicodem, J.A. João, Photoisomerization of chalcone: wavelength dependence, J. Photochem. 15 (3) (1981) 193–202, doi:10.1016/0047-2670(81)87003-7.
[59] R. Zhang, M. Wang, H. Sun, A. Khan, R. Usman, S. Wang, X. Gu, J. Wang, C. Xu, Effect of configurational isomerism and polymorphism on chalcone fluorescent properties, New J. Chem. 40 (2016) 6441–6450, doi:10.1039/c6nj00976j.
[60] N.S.A.Razak Mahesha, N.S.A. Razak, J. Jamalis, M.V. Deepa Urs, N.S. Lingegowda, K. Raghava Reddy, N.K. Lokanath, S. Naveen, Synthesis, characterization, crystal structure and theoretical simulation of novel ethyl 2-(7-hydroxy-4-methyl-2-oxo-2H-chromen-3-yl)acetate, Chem. Data Collect. 28 (2020) 100425, doi:10.1016/j.cdc.2020.100425.
[61] R. Zhang, M. Wang, H. Sun, A. Khan, R. Usman, S. Wang, X. Gu, J. Wang, C. Xu, Effect of configurational isomerism and polymorphism on chalcone fluorescent properties, New J. Chem. 40 (7) (2016) 6441–6450, doi:10.1039/c6nj00976j.
[62] M.A. Alsafi, D.L. Hughes, M.A. Said, First COVID-19 molecular docking with a chalcone-based compound: synthesis, single-crystal structure and Hirshfeld surface analysis study, Acta Cryst. C: Struct. Chem. 76 (12) (2020) 1043–1050.
[63] D. Dey, S.P. Thomas, M.A. Spackman, D. Chopra, Quasi-isostructural polymorphism" in molecular crystals: inputs from interaction hierarchy and energy frameworks, Chem. Commun. 52 (10) (2016) 2141–2144, doi:10.1039/c5cc09741j.
[64] C.S. Karthik, K. Kumara, S. Naveen, L. Mallesha, P. Mallu, M.V. Deepa Urs, N.K. Lokanath, Thermal, optical, etching, structural studies and theoretical calculations of [1-(2, 5-Dichloro-benzenesulfonyl)-piperidin-4-yl]-(2,4-difluorophenyl)-methanone oxime, J. Mol. Struct. 1224 (2021) 129077, doi:10.1016/j.molstruc.2020.129077.
[65] S. Naveen, K. Kumara, A.D. Kumar, K.A. Kumar, A. Zarrouk, I. Warad, N.K. Lokanath, Synthesis, characterization, crystal structure, Hirshfeld surface analysis, antioxidant properties and DFT calculations of a novel pyrazole derivative: ethyl 1-(2,4-dimethylphenyl)-3-methyl-5-phenyl-1H-pyrazole-4-carboxylate, J. Mol. Struct. 1226 (2021) 129350, doi:10.1016/j.molstruc.2020.129350.
[66] B. Pramodh, P. Naresh, S. Naveen, N.K. Lokanath, S. Ganguly, J. Panda, S. Murugesan, A.V. Raghu, I. Warad, Synthesis, spectral characterization, crystal structure and theoretical investigation of (E)-3-(4-bromothiophen-2-yl)-1-(5-bromothiophen-2-yl)prop-2-en-1-one, Chem. Data Collect. 31 (2020) 100587, doi:10.1016/j.cdc.2020.100587.
[67] B. Pramodh, N.K. Lokanath, S. Naveen, P. Naresh, S. Ganguly, J. Panda, Molecular structure, Hirshfeld surface analysis, theoretical investigations and nonlinear optical properties of a novel crystalline chalcone derivative: (E)-1-(5-bromothiophen-2-yl)-3-(p-tolyl)prop-2-en-1-one, J. Mol. Struct. 1161 (2018) 9–17, doi:10.1016/j.molstruc.2018.01.078.
[68] N.K. Nkungli, J.N. Ghogomu, Theoretical analysis of the binding of iron(III) protoporphyrin IX to 4-methoxyacetophenone thiosemicarbazone via DFT-D3, MEP, QTAIM, NCI, ELF, and LOL studies, J. Mol. Model. 23 (7) (2017), doi:10.1007/s00894-017-3370-4.